JOURNAL OF SOLID STATE CHEMISTRY 103, 81–94 (1993)

The Thermochromic Vanadium Dioxide

I. Role of Stresses and Substitution on Switching Properties

J. C. RAKOTONIAINA,*,† R. MOKRANI-TAMELLIN,*
J. R. GAVARRI,*,[1] G. VACQUIER,† A. CASALOT,†
AND G. CALVARIN‡

**Laboratoire des Matériaux Multiphasés et Interfaces, ex-LMPV, Université de Toulon et du Var, BP 132, 83957 La Garde Cedex, France; †Equipe de Chimie du Solide, Laboratoire de Physico-Chimie des Matériaux, Université de Provence, Centre Scientifique St-Charles, 13331 Marseille Cedex 03, France; and ‡Laboratoire de Chimie-Physique des Solides, Ecole Centrale des Arts et Manufactures, 92295 Chatenay-Malabry, France*

Received July 4, 1992; in revised form July 24, 1992; accepted August 4, 1992

The monoclinic ⇔ tetragonal transition occurring at 341 K for VO_2 vanadium dioxide and the corresponding switching of the optical properties can be affected in various ways by thermal treatments, substitution, and pressure. The transition in pure or substituted powdered samples is characterized by thermal analysis (DSC), X-ray (XRD) and neutron (NRD) diffractions, and infrared spectroscopy (IR). The influence of pressure on the transition is discussed from neutron diffraction experiments at high pressure. The anisotropic compressibility coefficients in the monoclinic and tetragonal phases are considered. Some kinetic effects close to T_c, the transition temperature, have been observed by X-ray diffraction. The influences of pressure and substitution on the transition are then interpreted from a classical description of the chemical bonds in VO_2.

I. Introduction

The general aim of this study is to test thermochromic VO_2 oxides for coating applications. VO_2 vanadium oxide is well known for its monoclinic to tetragonal structural transition at $T_c = 341$ K. Many studies of the properties linked with the VO_2 structural and electronic changes are available in the literature (*1–4*). This crystallographic transition is accompanied by a strong variation in conductivity, magnetic, and specific heat properties (*5–15*). The insulator state in VO_2 can be associated with pairing of the single d electrons of two neighboring vanadium atoms. The basic metal orbitals are of d^2sp^3-type with one d orbital having one electron and two d orbitals available for π bonding. In the insulating state, the gap between full valency t bands and empty t^* or π^* bands ($E_g = 0.7$ eV) was extensively explained in the literature (*16*). The metal state might be described as resulting from vanishing of such a gap.

Optical properties (*17*) exhibit again interesting variations in the range of infrared wavelengths (1 to 50 μm). The band structure change involves a strong perturbation in optical transmittance T_r.

Several recently published papers on VO_2

[1] To whom correspondence should be addressed.

0022-4596/93 $5.00

layers deposited on various substrates have revealed some unexplained influence of these substrates on them (*18–23*).

Generally, chemical substitution is used as a good tool for modifying the properties of a material through the electron valency changes or pure size effects due to the substitution (*24–26*). Under certain circumstances, the latter effects might be considered as pressure effects and consequently, the Clausius–Clapeyron relation can be a useful tool for a systematic interpretation and prediction of the variations of the T_c transition temperature as a function of dopants or defects (*27, 28*). This is not the case if valency changes may occur for both host and substituting cations. For a cationic substitution of M (IV) ions by M' (IV) cations, an electronic exchange can be observed with $m > 4$:

$$(m - 4)M^{4+} + M^{4+} = M'^{m+} + (m - 4)M^{3+}. \quad \text{(I)}$$

We report here some new results concerning the influence of pressure and tungsten substitution for vanadium on the T_c transition temperature in the case of polycrystalline materials.

II. Experimental Process

II.1. Preparation of the Samples

The preparation of tungsten-substituted VO_2 under powder form has been first considered using dry processes (solid-state reactions). Two main routes were primarily investigated.

The first route corresponds to a direct synthesis from VO_2 and WO_2 mixtures:

$$xWO_2 + (1 - x)VO_2 = V_{1-x}W_xO_2. \quad \text{(II)}$$

The mixed oxides are heated in initially evacuated quartz ampoules close to 875 K. VO_2 is classically obtained after stoichiometric reaction between V_2O_5 and V_2O_3 at 875 K (*29*).

The second route corresponds to use of W, V_2O_3, V_2O_5, and WO_3 mixtures, under chemical conditions resulting from the tungsten amount:

—for $x < 0.20$:

$$xW + \frac{1 + 3x}{4}V_2O_5 + \frac{1 - 5x}{4}V_2O_3 = V_{1-x}W_xO_2. \quad \text{(IIIa)}$$

—for $x > 0.20$:

$$\frac{x}{3}W + \frac{1 - x}{4}V_2O_5 + \frac{1 - x}{4}V_2O_3 + \frac{2x}{3}WO_3 = V_{1-x}W_xO_2. \quad \text{(IIIb)}$$

V_2O_3 is obtained by reduction of V_2O_5 by hydrogen at a temperature close to 875 K (*29*). Heating in evacuated silica tubes at 925 K (the T_m oxide melting-points are $T_m \approx 945$ K for V_2O_5 and $T_m \approx 2230$ K for V_2O_3) and annealing at 1075 K have permitted us to obtain well defined samples of solid solutions $V_{1-x}W_xO_2$. In fact, it is necessary to achieve several cyclings: heating (1075 K), cooling, then grinding. For high substitution levels ($0.1 < x < 0.5$), the final crystal state can be quickly obtained, but this is not the case for low tungsten concentrations ($x < 0.05$). Some typical phases were obtained for the compositions $x = 0.20$, 0.25, 0.33, and 0.50. The phase system above $x = 0.50$ is so far not fully elucidated.

II.2. Thermal Analysis

The various pure and substituted samples have been investigated using differential scanning calorimetry (DSC) in the 290–420 K temperature range and under air atmosphere. A Setaram apparatus, equipped for analyses ranging between 77 and 773 K, was used.

The results, reported in Table I, for substituted samples with $x < 0.02$ reveal a strong decrease both in the transition temperature T_c and in the transition enthalpy

TABLE I

ENTHALPIES AND TEMPERATURES OF TRANSITION VS x COMPOSITION IN $V_{1-x}W_xO_2$ (D.S.C. ANALYSIS AT P = 1 bar IN THE RANGE 270–420 K)

x	0.000	0.005	0.010	0.015	0.020
Weight (mg)	45.30	32.20	31.80	44.40	48.00
ΔH_c (kJ · mol^{-1}) Relative error: 2%	4.23	3.40	3.07	2.04	1.91
T_c (DSC) (K) Absolute error: 0.1 K	339.0	325.0	312.6	298.7	282.5
T_c (XRD) (K) Absolute error: 0.5 K	341 (2)	323 (3)	315 (3)	295 (3)	280 (5)

Note. The T_c (DSC) temperatures are the so-called on-set temperatures which characterize the beginning of the transition. The T_c (XRD) temperatures are mentioned with absolute errors and measured when the tetragonal and monoclinic phases are both present in equivalent amounts on the XRD patterns.

ΔH_c. These results give an indication of the fact that low substitution levels of W induce a strong decrease in the efficiency of the transition. The $\delta T_c/\delta x$ ratio is found to be

$$\delta T_c/\delta x = -27.0 \times 10^2 \quad (\mathrm{K \cdot mol^{-1}}). \quad (2)$$

The experimental enthalpy variation law is

$$\Delta H_c = -4.20 - 1.43 \times 10^2 x + 3.16 \times 10^3 x^2 \quad (\mathrm{kJ \cdot mol^{-1}}), \quad (3)$$

which gives a ratio

$$\delta \Delta H_c/\delta x = -135.0 \quad (\mathrm{kJ \cdot mol^{-1}}).$$

Figure 1 represents the enthalpy variation for cycled samples in the composition range x = 0 to 0.020.

II.3. X-ray Diffraction Study of the Transition

Each sample has been investigated by X-ray diffraction on an automatized diffractometer (Siemens D 5000). Diffraction profiles have been analysed to determine the crystal quality of the samples.

The cell parameters of the monoclinic and tetragonal phases have been refined using preliminary graphic analysis (Socabim logicals) and a classical cell parameter refinement procedure.

Evidence of the transitions of the powder samples is given using first a heating house made sample holder then comparing the results with a standard experiment made in a heating X-ray diffraction camera (high angle resolution diffractometer).

The samples in the house made aluminium holder are directly surrounded by air and the temperature is obtained by direct heating of the metal holder (thermocouple in the sample). The calibration of temperature in the 290–400 K range is obtained using the well-known transition temperature of VO_2.

Some of the refined parameters are reported in Tables II (XRD and ND results) and III (substituted samples). The variation of the cell parameters (monoclinic or tetragonal) is represented in Fig. 2. It can be pointed out that, when substitution takes place, the cell parameters and the cell jumps at T_c are almost constant (except the a_M parameter linked with the rutile c_R axis).

A comparison with the thermal data (DSC) can be done in Fig. 3, where the variation of T_c (XRD) is reported. The experimental variation law is

$$T_c(x) = 338.2 - 2.65 \times 10^3 x \quad (\mathrm{K}). \quad (5)$$

For (V, W)O_2 samples, a temperature range in which two phases exist is observed

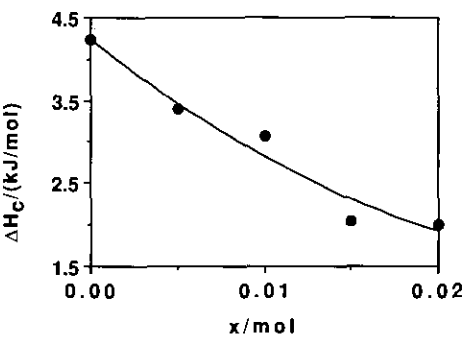

FIG. 1. Enthalpy of the transition from thermal analysis (DSC).

TABLE II

MONOCLINIC LATTICE PARAMETERS OF VO_2 AT DIFFERENT TEMPERATURES AND P = 1 (X-RAY DIFFRACTION = XRD) OR P = 10 kbar (NEUTRON DIFFRACTION = ND) ($a_M = 2c_R$; $b_M = a_R$; $c_M = b_R - c_R$)

Temperature (K)	a_M (pm)	b_M (pm)	c_M (pm)	β (degree)	$10^{30} \times V$ (m^3)
294.0 (XRD)	575.5 ± 0.3	452.5 ± 0.1	538.6 ± 0.3	122.61 ± 0.03	118.2 ± 0.2
295.0 (ND)	574.2 ± 0.4	452.1 ± 0.3	537.3 ± 0.4	122.60 ± 0.05	117.5 ± 0.2
315.0 (ND)	574.3 ± 0.4	451.9 ± 0.3	537.1 ± 0.4	122.58 ± 0.04	117.4 ± 0.2
323.0 (XRD)	575.6 ± 0.3	452.8 ± 0.1	538.6 ± 0.3	122.61 ± 0.03	118.2 ± 0.2
325.0 (ND)	574.0 ± 0.5	452.0 ± 0.3	537.2 ± 0.4	122.59 ± 0.05	117.4 ± 0.3
333.0 (XRD)	575.6 ± 0.3	452.7 ± 0.1	538.7 ± 0.3	122.62 ± 0.03	118.2 ± 0.2
335.0 (ND)	574.5 ± 0.4	451.9 ± 0.3	537.3 ± 0.4	122.60 ± 0.04	117.5 ± 0.2
343.0 (XRD)	570.2 ± 0.3	455.6 ± 0.1	537.4 ± 0.3	122.04 ± 0.03	118.3 ± 0.2
345.0 (ND)	568.9 ± 0.5	454.6 ± 0.3	535.6 ± 0.4	122.01 ± 0.05	117.5 ± 0.2
353.0 (XRD)	570.4 ± 0.3	455.5 ± 0.1	537.4 ± 0.3	122.05 ± 0.02	118.4 ± 0.2
355.0 (ND)	570.4 ± 0.5	454.6 ± 0.4	535.7 ± 0.5	122.05 ± 0.05	117.4 ± 0.3
358.0 (XRD)	570.5 ± 0.3	455.5 ± 0.1	537.5 ± 0.2	122.06 ± 0.02	118.4 ± 0.1
393 K (ND; P = 1 bar)	575.2 ± 0.3	452.4 ± 0.1	538.0 ± 0.2	122.60 ± 0.03	118.0 ± 0.1

Note. Experimental corrections have been taken into account in the refinement procedure; the ND and XRD values have been obtained from different experiments without any calibration. The last ND data at 1 bar have allowed the direct calculation of compressibility coefficients. The compressibility of the high-temperature phase is calculated after calibration of the ND experiments to the XRD high-temperature experiments.

close to the transition temperature: the width of the transition is successively 5, 6, 10, and 15 K for the nominal compositions x = 0.005, 0.010, and 0.015. The very weak changes in cell parameters can be explained as follows:

1. In the metal state, at $T > T_c$, the W substitution is accompanied by a strong change in electron wavefunction.

2. In the semiconductor low-temperature phase, localized clusters of (W^{6+}, $2V^{3+}$) cations may be formed, but spread in the

TABLE III

MONOCLINIC LATTICE PARAMETERS OF $V_{1-x}W_xO_2$ AT 290 K (M = MONOCLINIC PHASE) AND 340 K (R = RUTILE PHASE) (X-RAY DIFFRACTION FOR P = 1 bar)

Composition $\times$ (mol^{-1})		a_M (pm)	b_M (pm)	c_M (pm)	β (degree)	$10^{30} \times V$ (m^3)
0.005	M	575.5 ± 0.9	452.2 ± 0.5	538.2 ± 0.9	122.6 ± 0.1	117.8 ± 0.6
	R	570.4	455.6	537.6	122.1	118.4
0.10	M	575.2 ± 0.6	452.6 ± 0.3	537.7 ± 0.6	122.6 ± 0.1	117.9 ± 0.3
	R	570.6	455.4	537.5	122.1	118.3
0.015	M	576.2 ± 0.7	453.2 ± 0.3	538.7 ± 0.7	122.7 ± 0.1	118.4 ± 0.4
	R	570.6	455.6	537.3	122.1	118.4
0.020	M	570.6 ± 0.2	455.8 ± 0.1	537.7 ± 0.3	122.0 ± 0.1	118.5 ± 0.1
	R	571.1	455.8	537.8	122.1	118.6

Note. The parameters at 340 K (symbol R) of the high-temperature phase are given in the monoclinic cell representation.

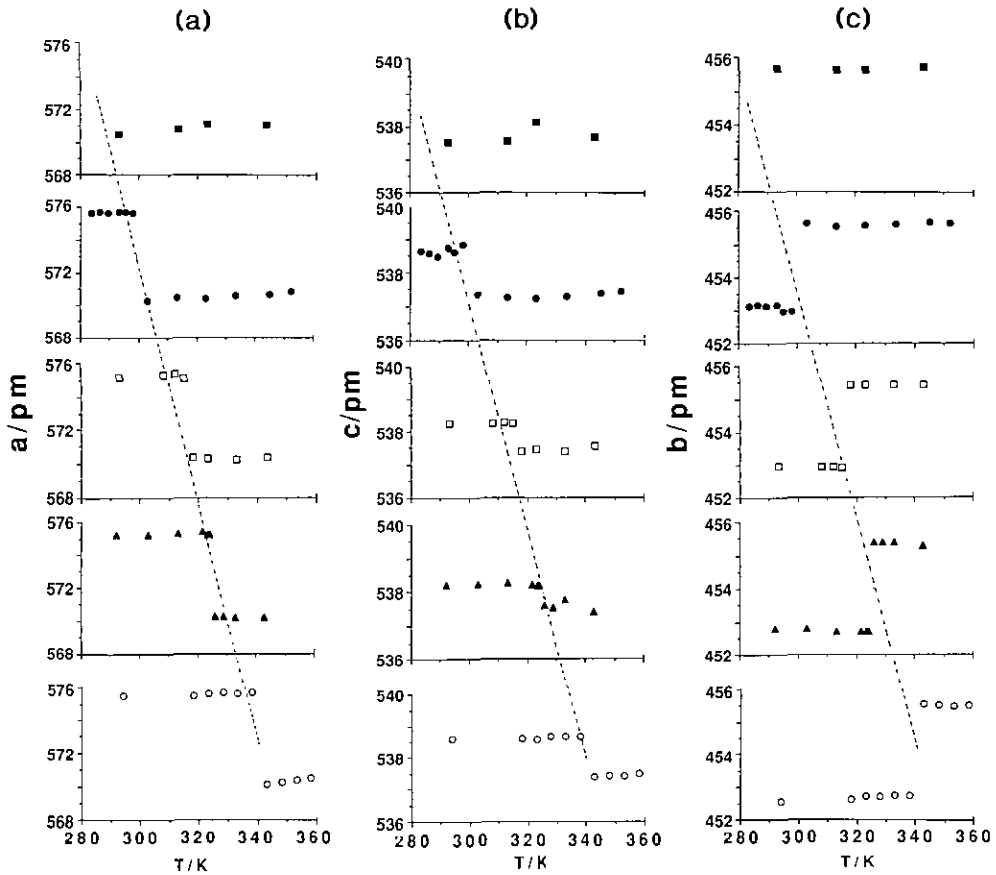

FIG. 2. Monoclinic cell characteristics as a function of x tungsten concentration: (a) a_M parameter, (b) b_M parameter, (c) c_M parameter. For all figures the x values are indicated as: ○, $x = 0.000$; ▲, $x = 0.005$; □, $x = 0.010$; ●, $x = 0.015$; ■, $x = 0.020$; The dotted line represents $\delta T_c/\delta x = -2.7 \times 10^3$ K · mol^{-1}.

lattice; electrons are localized in bonds, the average lattice observed by X-ray diffraction is predominantly that of pure VO_2 domains (>98% in volume).

On the other hand, some kinetic effects have been shown in the 333–341 K temperature range and below the transition (Fig. 4). Close to the two first Bragg peaks $(111)_M$ and $(011)_M$, one small peak (noted S) that does not belong to the monoclinic or rutile lattices can be observed; it disappears above the transition temperature but its existence is not systematic after cycling. This transient feature is not clearly understood. Two interpretations might be proposed:

1. The appearance of a new structure linked with domain walls due to phase–antiphase domains or pretransitional effects: a monoclinic distortion of the tetragonal phase might be in agreement with such peaks, but it is not possible to conclude definitely.

2. The appearance of a modulation below the transition and conditioned by the martensitic character of the phase change (first-order transition).

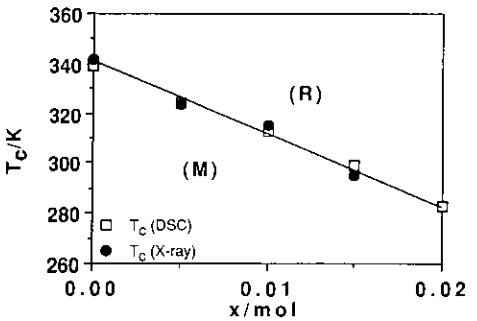

FIG. 3. Variation of T_c as a function of x (XRD and DSC).

In both cases the kinetics of the transition seems to be connected with such pretransitional effects.

The transition point was investigated in details by the simultaneous presence of the peaks of the monoclinic and tetragonal phases on the diffraction patterns. In Fig. 4, both low- and high-temperature phases are shown with the two new small additional peaks. In all experiments carried out at the transition point, a systematic evolution of the intensities, but not of the angular positions, was observed when the temperature was kept constant (±0.1 K). By heating the transition is found to be at 341.3 K, while by cooling it moves down to 339 K. This hysteresis is less significant than that observed during thermal analysis experiments (for DSC experiments it is about 8 K).

Better understanding of such time dependent features might be of high interest to control the optical behaviors for thermochromic applications conditioned by thermal cycles.

II.4. Neutron Diffraction at High Pressure

Several experiments under high pressure and at various temperatures on a pure VO_2 sample were carried out at the I.L.L. in Grenoble, using a high-resolution angle diffractometer D_{1A}.

The sample was put into a special cell under 1 bar and 10 kbar as hydrostatic pressures. In that experiment, only the lattice of the oxygen atoms could be observed (the coherent scattering length of a vanadium atom is zero in the case of neutron diffraction). The cell parameters at 10 kbar have been analysed at temperatures varying from 290 to 353 K, surrounding thus the transition point. In Table II the cell parameters are reported and a comparison with XRD results can be done.

The mean compressibility coefficients of the monoclinic and tetragonal phases have been calculated from the cell parameters ($a_M = 2c_R$; $b_M = a_R$; $c_M = b_R - c_R$) at, respectively, $T_1 = 290$ K $< T_c$ and $T_2 = 350$ K $> T_c$. In Table IV, the volume compressibility,

$$\chi_V = -\frac{1}{V}\cdot\frac{\partial V}{\partial P}, \tag{6}$$

and its linear components χ_{iM} in the monoclinic low-temperature phase and χ_{iR} in the rutile high-temperature phase

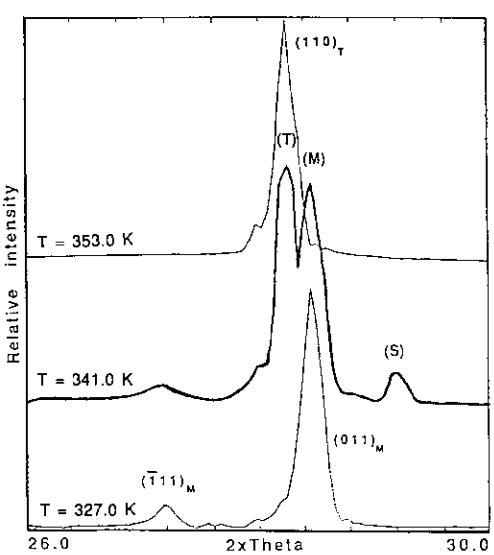

FIG. 4. Additional peaks or satellites observed from 333 K to T_c and disappearing above T_c in pure samples.

TABLE IV

COMPRESSIBILITY COEFFICIENTS (IN 10^{-12} Pa^{-1})

Monoclinic cell $T_1 < T_c$	Tetragonal cell $T_2 > T_c$
$\chi_{1M}[001] = 1.74$	$\chi_{1R} = 2.30$
$\chi_{2M}[100] = 0.66$	$\chi_{2R} = 2.40$
$\chi_{3M}[101] = 1.49$	
$\chi_V = 4.00\ (0.4)$	$\chi_V = 7.10\ (0.7)$

Note. The crystal directions of the rutile packing are noted [*uvw*]. The relative errors are about 10%.

$$\chi_{1M} = -\frac{1}{a_M}\cdot\frac{\partial a_M}{\partial P} \quad (7a)$$

$$\chi_{2M} = -\frac{1}{b_M}\cdot\frac{\partial b_M}{\partial P} \quad (7b)$$

$$\chi_{3M} = -\frac{1}{c_M}\cdot\frac{\partial c_M}{\partial P} \quad (7c)$$

$$\chi_{1R} = -\frac{1}{a_R}\cdot\frac{\partial a_R}{\partial P} \quad (7d)$$

$$\chi_{2R} = -\frac{1}{c_R}\cdot\frac{\partial c_R}{\partial P} \quad (7e)$$

are reported (in 10^{-12} Pa^{-1}).

A strong anisotropy is observed for the monoclinic structure with a [001] direction (pseudo-rutile c_R axis) more compressible than the [100] one. In the high-temperature phase, always more compressible than the low-temperature one, the linear coefficients increase strongly, χ_{1R} and χ_{2R} becoming equal. Such a change in elastic properties has to be directly associated with the electronic and structural changes with a strong modification in chemical bonds. It is interesting to note that a similar anomaly is observed on thermal expansion with a thermal expansion strongly weaker below the transition temperature than above T_c.

The crystallographic changes at T_c and under 10 kbar can be characterized and then compared with those observed under the ambient pressure of 1 bar. In the [100] and [001] directions of the rutile structure (a_R, c_R) the following cell parameter jumps have respectively been observed at 1 bar and 10 kbar:

$$[100] \quad (a_R - b_M) = +2.5 \text{ pm}, \quad (a_R - b_M) = +2.1 \text{ pm}; \quad (8a)$$

$$[001] \quad \frac{(2c_R - a_M)}{2} = -2.8 \text{ pm}, \quad \frac{(2c_R - a_M)}{2} = -2.7 \text{ pm}. \quad (8b)$$

Thus the effect of pressure on the transition is anisotropic:

1. Along the rutile [001] axis, at a pressure of 10 kbar, the transition jump is approximately unchanged.

2. In the square plane of the rutile cell, such a pressure induces a decrease in the transition jump.

These results allow us to expect a small decrease in the transition enthalpy involving a limited decrease in the quality of the transition, i.e., in the interesting switching effects. They clearly show that the transition amplitude is moderately affected by stresses, i.e., anisotropic stresses from host lattices or substrates at the interfaces (grain boundaries).

II.5. Infrared Spectroscopy

The change in optical transmittance T_r, characteristic of the thermochromic behavior of our polycristalline samples VO_2, was analyzed using a Perkin–Elmer 559 B spectrophotometer in the range 4000–250 cm^{-1}.

The samples were classical KBr pellets, including powdered pure VO_2 (0.1 wt%) initially ground to obtain very fine particles. They had been placed in a house made heating sample holder. The temperature could vary between room temperature and 400 K. The thickness of the pellets was roughly 0.1

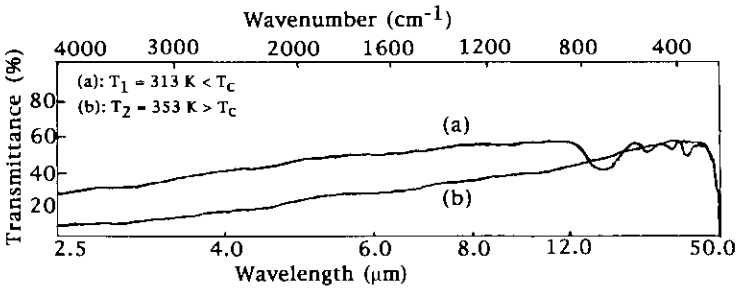

FIG. 5. Transmittance spectra in the 2.5–50 μm wavelength range for a KBr pellet having 0.1% of VO_2 as pigment: (a) T_r (LT), (b) T_r (HT). At low temperature the vibrational bands are clearly characterized by a V–O stretching mode at about 700 cm^{-1}.

mm. At the T_c transition temperature, it was possible to quickly cool or reheat the sample using air flux.

Many cycles were carried out; they have shown a good reproducibility of the results, the transmittance behavior being different for the LT monoclinic phase and for the HT rutile phase. The typical optical transmittance spectra of these phases are reported, in Fig. 5, for an incident wavelength varying between 2.5 and 40 μm for T_1 = 313 K and T_2 = 353 K. They give evidence of some characteristic features:

1. Above the transition temperature T_c, it appears a strong, but quite regular, decrease of the transmittance T_r in the range 2.5 to 12 μm. A ΔT_r jump occurs within a small temperature range of about 10 K, essentially due to the thermal gradient. This evolution results from the appearance of the metal state at high temperature.

2. An important modification is observed in the 12–40 μm range. Some vibrational frequency absorption bands (750–670, 530–510, 450–420, 360–320 cm^{-1}) are clearly visible at low temperature. They cannot appear at high temperature due to formation of a metallic behavior.

Then, W-dopped VO_2 transmittance has been investigated as a function of x ($x \in [0; 0, 02]$. An optical transition is observed when the structural transition occurs. Using the experimental values obtained for transmittance above and under the transition, it is possible to compare the various switching effects for one wavelength (2.5 μm).

In Fig. 6, the relative variation law is then

$$\Delta T_r(x) = T_r(\mathrm{LT}, x) - T_r(\mathrm{HT}, x) = 0.14 \exp(-105x). \quad (9)$$

III. Discussion

III.1. Substitution by W^{6+} Cations

In order to characterize the structural influence of the tungsten substitution, we have

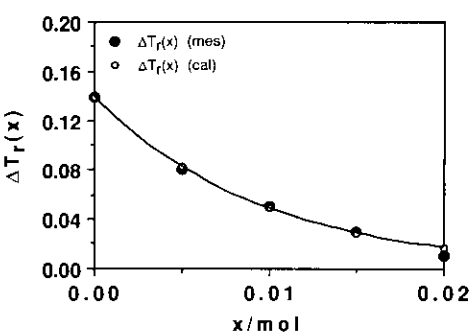

FIG. 6. Variation of transmittance with x at λ = 2.5 μm. A comparison of $T_{r(x)}$ is given, for each x value, between the monoclinic (LT) and rutile (HT) phases.

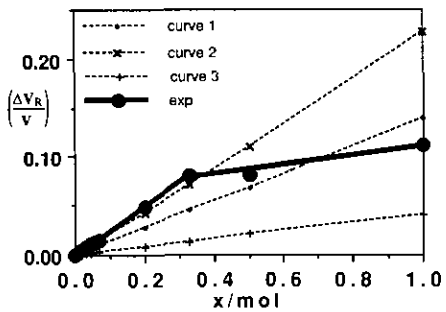

FIG. 7. Modeling of the cell volume for the solid solution. The best fit is represented under the model 2 (curves 2 and 3); it is compared to the model 1 calculation using the uncorrect hypothesis of the sole substitution by W^{4+} cations (curve 1 or (A) chemical formula). The experimental $V(x)$ function has been obtained from both literature data and our own results (large black circles).

plotted the relative cell volume variation in Fig. 7 with

$$\frac{\Delta V_R}{V} = \frac{V_R(x) - V_0}{V_0}, \qquad (11)$$

where $V_R(x)$ is the experimental volume obtained from both literature data and our own results for the tetragonal high-temperature phase and V_0 the hypothetical volume of pure VO_2 described in a pseudo-rutile form at 300 K. A clear change is observed in the slope of the curve $\Delta V_R/V = f(x)$. It can be easily explained, in full agreement with previous works (*30*), using simple geometrical considerations.

For our approach, we must suppose that, along the $V_{1-x}W_xO_2$ solid solution, all d_{V-O} metal–oxygen distances are quite similar for a given x value. This proposal is correct in rutile pure VO_2 where each vanadium is surrounded by six oxygen atoms, four at $d_1 = 192.4$ pm and two at $d_2 = 192.9$ pm, giving a mean value of $d_0 = 192.6$ pm). So it is possible to consider a linear relation between the average value d_{V-O} and the experimental d values corresponding to the V^{4+}–O ($d_{V^4} = 192.6$ pm), V^{3+}–O ($d_{V^3} = 200.0$ pm), W^{6+}–O ($d_{W^6} = 193.0$ pm), W^{4+}–O ($d_{W^4} = 199.0$ pm) bonds included in the solid solutions.

For $x < 0.333$ one can use the linear relation

$$d_{V-O} = (1 - 3x) \cdot d_{V^4} + 2x \cdot d_{V^3} + x \cdot d_{W^6}. \qquad (12a)$$

For $x > 0.333$ the relation is

$$d_{V-O} = \frac{3x - 1}{2} \cdot d_{W^4} + (1 - x) \cdot d_{V^3} + \frac{1 - x}{2} \cdot d_{W^6}. \qquad (12b)$$

The HT-phase parameters can then be written in connection with the O–V–O angle, called ϕ, (taken equal to 90°) in the $(110)_R$ plane,

$$a_R(x) = \sqrt{2} d_{V-O} \cdot \left[1 + \sin\left(\frac{\phi}{2}\right)\right] = k_1 \cdot d_{V-O}, \qquad (13a)$$

$$c_R(x) = 2 d_{V-O} \cdot \cos\left(\frac{\phi}{2}\right) = k_2 \cdot d_{V-O}, \qquad (13b)$$

giving the general expression of a tetragonal cell volume:

$$V_R(x) = k_1^2 \cdot k_2 \cdot d_{V-O}^3. \qquad (14)$$

For the evaluation of the mean M–O bond length as a function of x, we have to consider two kinds of oxidation states for cations:

1. The normal oxidation states of vanadium and tungsten cations which are present in the rutile compounds might be +4; if this is true, the electronic formula of the solid solution should be written as follows (with an (A) chemical formula):

$$V^{4+}_{1-x}W^{4+}_x O^{2-}_2. \qquad (A)$$

2. However, the above oxidation states cannot remain constant (see the chemical relation (1)). In our case, the typical electronic transfer is

$$2V^{4+} + W^{4+} = W^{6+} + 2V^{3+}, \quad \text{(IV)}$$

which corresponds to the (B) chemical formula,

$$V_{2x}^{3+}V_{1-3x}^{4+}W_x^{6+}O_2^{2-}, \quad \text{(B)}$$

the possibility of which being limited to an $x \leq 0.33$ domain. Above this border limit value W^{4+} and W^{6+} ions are both present, giving the (C) chemical formula

$$V_{1-x}^{3+}W_{\frac{3x-1}{2}}^{4+}W_{\frac{1-x}{2}}^{6+}O_2^{2-}, \quad \text{(C)}$$

which can be written as (D) chemical formula

$$W_{\frac{3x-1}{2}}^{4+}[V_2^{3+}W^{6+}]_{\frac{1-x}{2}}O_2^{2-}, \quad \text{(D)}$$

where V_2W clusters are supposed to be present: such a notation is supported by the fact that a phase V_2WO_6 has already been prepared (*31*).

It is possible to obtain the expressions of Eq. (14) for each chemical formula (A), (B), and (C) and to plot them in Fig. 7 (respectively represented by curves 1, 2, and 3). In Fig. 7 a quite good agreement is obtained between the experimental function and a modelized one based on redox reactions between vanadium and tungsten cations (curves 2 and 3). Such conclusions are in full agreement with recent publications (*30, 32, 33*) in which the authors gave evidence of W^{6+}–O bonds and W^{6+}–V^{3+} pairs.

III.2. Prevision of the Influence of Stresses

Influence of the interfaces. In the case of VO_2 thin layers, the stresses at the interfaces have generally been considered as high enough (*34*). A simple approximation for such stresses σ can be obtained from the relation

$$\sigma = e \cdot E, \quad (15)$$

with E being the appropriate elastic constant and e the deformation due to the difference in interatomic distances between VO_2 and the substrate after cooling (or quenching) from synthesis temperature to room temperature.

A good value of e can be evaluated from the α_i thermal expansion coefficients of the two materials (substrate and coating)

$$e = (\alpha_{sub} - \alpha_{coa}) \cdot [T_{up} - T_{low}], \quad (16)$$

where T_{up} is the high temperature reached by the materials during deposition ($T_{up} \approx 773$ K) and T_{low} is the low temperature after cooling or quenching (under these conditions, $e \in [0.04\text{–}0.08]$).

An indication of the E value can be obtained from the compressibility measurements considering that it is approximately of the same order as the reciprocal compressibility coefficients of the crystal. In our case, E will be taken equal to $\chi^{-1} = 2.5 \times 10^{11}$ Pa.

So we can consider that the interface stresses are about $S = 10\text{–}20$ kbar. They might affect the transition by decreasing its amplitude and thus damaging the efficiency of the material. For VO_2, previous data show a pressure dependence of T_c (*35*):

$$\frac{\delta T_c}{\partial P} \approx -5 \times 10^{-4} \quad (\text{K} \cdot \text{bar}^{-1}). \quad (17)$$

So, for a finite increase of pressure equal to the E minimum value ($\Delta P = +10$ kbar), we have to expect a decrease in the transition temperature $\Delta T_c = -5$ K.

Influence of atomic size. A tentative approach is now possible again to understand the complex influence of pressure and substitution on switching optical properties. In the case of stable 4+ cations (i.e., Ti^{4+}) the role of the cation size can be compared to an internal pressure effect.

When the radius of the substituting cation is larger than that of the host cation, the pressure changing is positive ($\delta P > 0$). So, as $\delta T_c/\delta P$ is negative, it is possible to predict

that the transition temperature will be lowered.

For unstable cations (W^{4+}, Nb^{4+}, ...) the role of the cation size is negligible: that of the electron transfer (doping level) is prominent, at low temperature, with formation of V^{3+} and W^{6+} (or Nb^{5+}) ions (*36*, *37*). In that case, the substitution of 1% of V by W atoms in the VO_2 lattice corresponds to 3% of global defects. With our own determination of the transition temperature decrease in the case of a W substitution, the composition dependence of T_c has been given by Eq. (2).

Using elastic approximations it is now possible to distinguish the influences of size effects and electron doping. For a W substitution, and taking into account that both V^{3+} and W^{6+} cations are present, the local stress σ can be given by the approximate relation

$$\sigma = C \cdot \frac{\Delta d}{d}, \qquad (18)$$

where C represents a local elastic data.

Using the hypothesis that the C value has to be identified to the E one, and considering simultaneously our compressibility measurements ($E \approx 2.5.10^{+11}$ Pa), the mean bond length in the HT phase ($d = 200$ pm) and its variation due to foreign cations ($\Delta d = 5$ pm), the local σ value might be about $\sigma = 120$ kbar. However, the σ value resulting from this approximation has to be corrected to involve the mean composition in W. For a composition $x = 0.010$ (1% W), the $\Delta P \approx \sigma$ value would only be 1.2 kbar: the resulting transition temperature change should be $\Delta T_c = -0.6$ K instead of $\Delta T_c = -27$ K as observed here.

This well illustrates the prominent role of electron transfer in the transition temperature variations.

III.3. Modeling of the Transition

Within the classical model proposed by Goodenough (*25*), the five d orbitals of V^{4+} cation can be considered as bound to oxygen ones in the following couplings:

—σ and π couplings are generated respectively from the $d_{zy} + d_{x^2}$ orbitals and from the d_{zx} and d_{xy} orbitals of V^{4+}.

—one V–V coupling noted $d\|$ (or t_{2g} band) is generated using the last $d_{z^2-y^2}$ orbital of the next neighboring V^{4+} cations along the chains of octahedra parallel to the rutile c_R axis.

This last coupling is directly at the origin of the metal behaviour of the rutile phase.

In the monoclinic phase the distortions of chemical bonds V–O and V–V are illustrated in Fig. 8 by an irregular environment of the V_1 atom with very different bonds (*16*, *38*):

—single bonding with V_1–O_1' = 205 pm, V_1–O_2 = 201 pm, V_1–O_3 = 203 pm

—twofold bonding with V_1–O_1 = 176 pm

—mixed bonding with intermediate distances V_1–O_2 = 187 pm and V_1–O_3 = 186 pm.

In the crystal, there is a π delocalization centered on four atoms V_1–O_2–V_1'–O_3; in Fig. 8, it is represented by dotted circles.

As a consequence, alternate zones noted (+) or (−) clearly appear: the symbol (+) permits to visualize the π delocalization. In the neighboring chain, the same alternative (+) and (−) zones are present: however, due to the rutile structure, a shift clearly appears along the c_R rutile axis.

Such a representation gives a direct evidence for two possible sequences of distortions in the rutile structure:

1. Along the rutile c_R axis, alternative (+) and (−) zones and direct V–V bonds induce the 2-X superstructure vector:

$$a_M = 2c_R.$$

2. In the $(a_R + b_R)$ direction, i.e., in the plane perpendicular to c_R axis, such alternative (+) and (−) zones induce a new period corresponding to two vectors:

$$b_M = a_R \quad \text{and} \quad c_M = a_R - c_R.$$

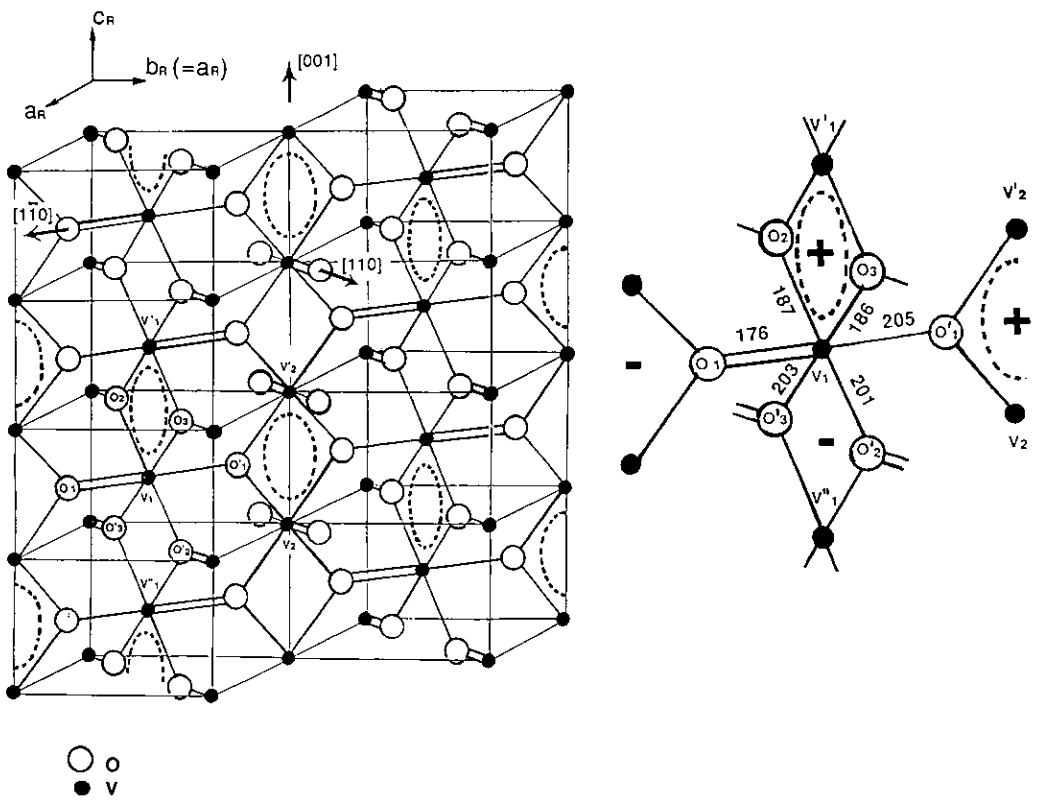

FIG. 8. Chemical bonds in the rutile type related structure of VO_2 at $T < T_c$. Plane representation of chemical bond arrangements with (+) and (−) zones. The (+) zones are those in which double bonding can occur. The superstructure is then evidenced using the dotted circle periodicity. Distances are given in pm.

Such a model is in full agreement with the experiments. It can be applied to all our present observations.

When thermal activation occurs with increasing temperature up to T_c, the change in electron distribution may correspond to a delocalization of the V–V bonds along the c_R axis (in fact the splitted $t\|$ and t^* bands are changed into a single band which leads to metallic behavior).

If it is assumed that the double bonds associated with the covalent V–V bonds induce a distortion of the oxygen octahedra in the c_R direction (change in V–O=V angle), the strong decrease in the a_M parameter and the strong increase in b_M correspond to vanishing of such distortions in the metallic state.

In other words, in the chains along the rutile c_R axis, some octahedra are abnormally elongated at $T < T_c$, thus involving direct contact between oxygen in the $[101]_R$ rutile structure directions; for $T > T_c$ the octahedra are regular and no short O–O distance is present.

Such a description allows better understanding of the present experimental variation,

$$\Delta a_M = -2\,\Delta b_M,$$

which is mainly due to the angular modification of octahedra.

In addition it is possible to interpret the variations of the elastic properties:

1. The pseudo-rutile c_R axis is more compressible in the low-temperature phase than in the high-temperature phase, because some oxygen octahedra (those of the (−) zone) are abnormally elongated in the insulating phase.

2. As a consequence of these distortions, the rutile $[100]_R$ directions are less compressible because of the existence of short O–O and V–V distances.

3. In the metal state, octahedra are regular: no abnormal repulsive short O–O distance is observed. Thus the average compressibility coefficients of the rutile lattice may be expected to exceed those of the insulating phase.

IV. Conclusion

In this investigation, it was clearly shown that the switching properties of the vanadium dioxide could strongly be modified by certain substituting cations. However, the substitution of V^{4+} by W^{6+} cations does not affect the cell parameter jumps at T_c, at least in the composition range $0 < x < 0.02$. Moreover, pressure effects including interface stresses or size effects due to substituted cations themselves are expected to be quite negligible.

The main feature observed in this study is the significant switching infrared transmittance of the 1% substituted samples ($x = 0.010$). In those conditions thermochromic substituted samples having a transition temperature T_c of 313 K, seems to be quite worthwhile for coating applications.

Another interesting feature must be now clarified: what is the exact origin of the additional satellites observed just below the transition temperature in pure VO_2 samples?

Acknowledgments

We gratefully acknowledge Dr. C. Vettier and Dr. A. W. Hewat, members of the Laue Langevin Institute in Grenoble, for helping us during neutron diffraction experiments; we also acknowledge Pr. A. Sebaoun and Dr. P. Satre, our colleagues at Toulon University, for their contribution during our thermal analysis measurements.

References

1. F. J. Morin, *Phys. Rev. Lett.* **3,** 34 (1959).
2. S. Westman, *Acta Chem. Scand.* **15,** 217 (1961).
3. J. Molenda and A. Stolklosa, *Solid State Ionics* **36,** 43 (1989).
4. S. Shin, S. Suga, M. Taniguchi, M. Fujisawa, H. Kanzaki, A. Fujimori, H. Daimon, Y. Ueda, K. Kosuge, and S. Kachi, *Phys. Rev. B* **41,** 4993 (1990).
5. K. Kosuge, Takada, and S. Kachi, *J. Phys. Soc. Jpn.* **18,** 318 (1963).
6. T. Kawakubo and T. Nakagawa, *J. Phys. Soc. Jpn.* **19,** 517 (1964).
7. A. S. Barker, Jr., H. W. Verleur, and H. J. Guggenheim, *Phys. Rev. Lett.* **17,** 1286 (1966).
8. G. Hyland, *J. Solid State Chem.* **2,** 318 (1970).
9. N. L. Levshin and S. Y. Poroïkov, *Fiz. Astron.* **31**(1), 93 (1990).
10. C. H. Neuman, A. W. Lawson, and R. F. Brown, *J. Chem. Phys.* **41,** 1591 (1964).
11. H. Sasaki and A. Watanabe, *J. Phys. Soc. Jpn.* **19,** 1748 (1964).
12. T. Ohashi and A. Watanabe, *J. Am. Ceram. Soc.* **49,** 519 (1966).
13. K. Kosuge, *J. Phys. Soc. Jpn.* **22,** 551 (1967).
14. G. J. Hill and R. H. Martin, *Phys. Rev. Lett. A* **27,** 34 (1968).
15. J. B. MacChesney and H. J. Guggenheim, *J. Phys. Chem. Solids* **30,** 225 (1969).
16. J. B. Goodenough, "Les oxydes des métaux de transition," 1ère ed., Gauthier-Villars, Paris (1973).
17. T. A. Hewston and M. P. Nadler, *J. Solid State Chem.* **71,** 278 (1987).
18. C. B. Greenberg, *Thin Solid Films* **110**(1), 73 (1983).
19. J. C. Lee, G. V. Jorgenson, and R. J. Lin, *Mater. Opt. Solar Energie Conv. Light. Technol.* **692,** 2 (1986).
20. S. M. Babulanam, T. S. Erikson, G. A. Niklasson, and C. G. Granqvist, *Mater. Opt. Solar Energie Conv. Light. Technol.* **692,** 8 (1986).
21. G. A. Nyberg and R. A. Burhrman, *Thin Solid Films* **147,** 111 (1987).
22. K. R. Speck, H. S. Whu, M. E. Sherwin, and R. S. Potember, *Thin Solid Films* **165,** 317 (1988).

23. J. F. De Natale, P. J. Hood, and A. B. Harker, *J. Appl. Phys.* **66,** 5844 (1989).
24. A. Akroune, Thèse, Université de Provence (1984).
25. J. B. Goodenough, *J. Solid State Chem.* **3,** 490 (1971).
26. M. Ritschel, N. Mattern, W. Brükner, H. Oppernam, G. Stover, W. Moldenhauer, J. Henke, and E. Wolf, *Krist. Teck.* **12,** 1221 (1977).
27. G. J. Hyland and A. W. B. Taylor, *J. Phys. Soc. Jpn.* **21,** 819 (1966).
28. K. V. Krishna Rao, S. V. Nagender Naidu, and L. Iyengar, *J. Phys. Soc. Jpn.* **23,** 1380 (1967).
29. G. Brauer, "Handbook of Preparative Inorganic Chemistry," 2nd ed., Vol. 2, p. 1421 (1965).
30. C. Tang, P. Georgopoulos, M. E. Fine, and J. B. Cohen, *Phys. Rev. B* **31,** 1000 (1985).
31. J. C. Bernier and P. Poix, *C. R. Acad. Sci. Paris* **265,** 1247 (1967).
32. W. Rudörff and H. Kornelson, *Rev. Chim. Miner.* **6,** 137 (1969).
33. J. Nii, M. Wakihara, and M. Taniguchi, *Mater. Res. Bull.* **15,** 945 (1980).
34. F. Cardillo Case, *J. Vac. Sci. Technol. A* **2,** 1509 (1984).
35. S. Minomura and H. Nagasaki, *J. Phys. Soc. Jpn.* **19,** 131 (1964).
36. A. Casalot, P. Dougier, and G. Villeneuve, "Séminaires de Chimie de l'Etat Solide," 6ème ed., Masson, Paris (1971).
37. P. Lederer, H. Launois, J. P. Pouget, A. Casalot, and G. Villeneuve, *J. Phys. Chem. Solids* **33,** 1969 (1972).
38. J. M. Longo and P. Kierkegaard, *Acta Chem. Scand.* **24,** 426 (1960).